Strong increase in the effective two-photon absorption cross-section of excitons in quantum dots due to the nonlinear interaction with localized plasmons in gold nanorods

Victor Krivenkov, Pavel Samokhvalov, Ana Sánchez-Iglesias, Marek Grzelczak, Igor Nabiev, Yury Rakovich

Nanoscale

Accepted Manuscript

This article can be cited before page numbers have been issued, to do this please use: Y. RAKOVICH , V. A. Krivenkov, P. Samokhvalov, A. Sánchez-Iglesias, M. Grzelczak and I. Nabiev, *Nanoscale*, 2021, DOI: 10.1039/D0NR08893E.

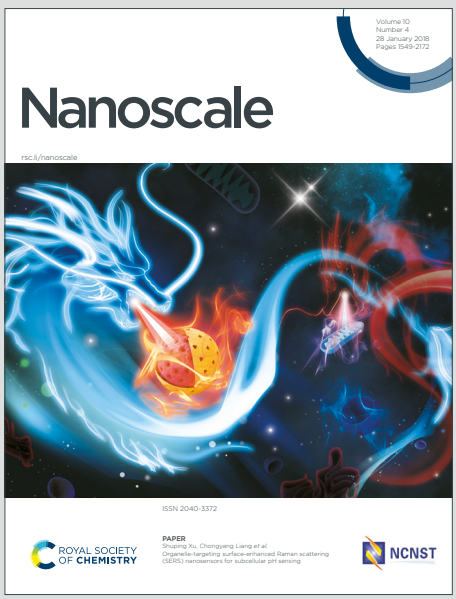

ROYAL SOCIETY OF CHEMISTRY

rsc.li/nanoscale

View Article Online
DOI: 10.1039/D0NR08893E

ARTICLE

Strong increase in the effective two-photon absorption cross-section of excitons in quantum dots due to the nonlinear interaction with localized plasmons in gold nanorods

Received 00th January 20xx,
Accepted 00th January 20xx

DOI: 10.1039/x0xx00000x

Victor Krivenkov,*[a] Pavel Samokhvalov,[a] Ana Sánchez-Iglesias,[b] Marek Grzelczak,[c,d,e] Igor Nabiev[a,f,h] and Yury Rakovich*[c,d,e,g]

Excitons in semiconductor quantum dots (QDs) feature high values of the two-photon absorption cross-sections (TPACSs), enabling applications of two-photon-excited photoluminescence (TPE PL) of QDs in biosensing and nonlinear optoelectronics. However, efficient TPE PL of QDs requires high-intensity laser fields, which limits these applications. There are two possible ways to increase the TPE PL of QDs: to increase their photoluminescence quantum yield (PL QY) or further increase the TPACS. Plasmonic nanoparticles (PNPs) may act as open nanocavities for increasing the PL QY via the Purcell effect, but this enhancement is strictly limited by the maximum possible QY value of 100%. Here we directly investigated the effect of PNPs on the effective TPACS of excitons in QDs. We have found that effective TPACS of excitons in a QD–PMMA thin film can be increased by a factor of up to 12 near the linearly excited gold nanorods (GNRs). Using gold nanospheres (GNSs), in which plasmons cannot be excited in the infrared range, as a control system, we have shown that, although both GNSs and GNRs increase the recombination rate of excitons, the TPACS is increased only in the case of GNRs. We believe that the observed effect of TPACS enhancement is a result of the nonlinear interaction of the plasmons in GNRs with excitons in QDs, which we have supported by numerical simulations. The results show the way to the rational design of the spectral features of plasmon–exciton hybrids to use them in biosensing and nonlinear optoelectronics.

Introduction

Semiconductor quantum dots (QDs) are known for their highly efficient two-photon absorption (TPA) compared to the conventional organic fluorophores.[1,2] Due to the very high values of two-photon absorption cross-sections (TPACSs),[3,4] QDs are widely used for two-photon fluorescent bioimaging,[5–7] where they ensure a uniquely high contrast, as well as for fabrication of nonlinear optoelectronic devices operating in the up-conversion mode.[8,9] However, due to the nonlinear nature of the TPA process, efficient two-photon excitation (TPE) of QD photoluminescence (PL) requires very high laser intensities,[2] which limits their applications. It is well known that the efficiency of the exciton PL in QD can be enhanced by coupling with plasmons in metal nanoparticles under single-photon excitation, which allows the use of lower radiation intensities for the excitation of PL.[10] This increase may be a result of the enhancement of the radiative recombination rate (the Purcell effect) due to the weak coupling of the emissive exciton transitions with plasmons and the correspondingly increased density of the photon states. Alternatively, this may be a result of the enhanced absorption.[11]

Regarding TPE PL, several studies have previously shown its strong enhancement in fluorescent organic dyes placed at the very short distances from metal nanostructures.[12–17] However, in these studies, the spectral conditions of the resonance between the plasmon modes and the fluorescence and absorption bands of the molecules were not specified, which made it difficult to correctly interpret the results. Therefore, the reported PL increase may have been related not only to the two-photon absorption enhancement, but also to an increase in the radiative recombination rate, also known as the Purcell effect.[18,19] In the case of the Purcell effect, the PL enhancement is not conditioned by the resonance of the excitation field with plasmon modes and, in general, can be achieved for both linear and nonlinear excitation. Commonly, the Purcell effect requires the resonance between the PL and plasmon bands for efficient plasmon–exciton coupling,[20–22] but the impact of the Purcell effect on the enhancement of TPE PL has been reported even for nonresonant interaction of organic molecules with plasmon nanoparticles (PNPs).[23] However, in the case of the Purcell

[a] National Research Nuclear University MEPhI (Moscow Engineering Physics Institute), Kashirskoe shosse 31, 115409 Moscow, Russian Federation
[b] CIC biomagune, Paseo de Miramón 182, 20014 Donostia - San Sebastián, Spain
[c] Centro de Física de Materiales (MPC, CSIC-UPV/EHU), Paseo Manuel de Lardizabal 5, 20018 Donostia - San Sebastián, Spain.
[d] Donostia International Physics Center (DIPC), Paseo Manuel de Lardizabal 4, 20018 Donostia-San Sebastián, Spain
[e] Polímeros y Materiales Avanzados: Física, Química y Tecnología, UPV-EHU, Paseo Manuel de Lardizabal 3, 20018 Donostia-San Sebastian, Spain
[f] Laboratoire de Recherche en Nanosciences (LRN-EA4682), Université de Reims Champagne-Ardenne, 51100 Reims, France.
[g] IKERBASQUE, Basque Foundation for Science, Maria Diaz de Haro 3, 48013 Bilbao, Spain
[h] I.M. Sechenov First Moscow State Medical University, Trubetskaya str. 8-2, 119992 Moscow, Russian Federation
* Corresponding authors
Electronic Supplementary Information (ESI) available. See DOI: 10.1039/x0xx00000x

effect, the overall PL enhancement strongly depends on the initial PL quantum yield (QY) of the fluorophore, and the results obtained for a specific fluorophore cannot be extrapolated to other types of emitters, which substantially limits the applicability of the obtained effect of PL enhancement.

Direct measurement of the plasmon-induced enhancement of two-photon absorption under controllable resonance conditions is an important task because the results obtained in such experiments will be independent of the fluorophore type. However, in the case of QD ensembles, it is rather challenging to distinguish the plasmon-induced TPACS enhancement from spontaneous emission modification due to the Purcell effect. The main reason is the strong quenching of QD PL near the metal surfaces and PNPs.[24] Moreover, the direct TPACS measurement techniques, such as z-scan, are also very limited for plasmon–exciton hybrids because of the extremely high linear absorptivity of metal nanoparticles themselves and inapplicability to optically thin samples.

To date, in all studies where TPE of QD PL near PNPs was obtained, only the PL intensity has been measured. In particular, efficient enhancement of the PL of single QD near single gold nanorod (GNRs) under TPE has been demonstrated.[25] However, in this case, the necessity of both the two-photon absorption enhancement and the change in the radiative recombination rate has been specifically emphasized. The PL enhancement under TPE has also been observed for individual epitaxial InGaN nanoparticles coated with a silver shell.[26] By reducing the temperature to 7K, the authors precluded the Purcell effect and also eliminated the quenching of QD PL near the metal. However, in this case, the role of the plasmon band position, as well as the degree of the PL enhancement at room temperature, remained unclear. Thus, there is a clear lack of studies on plasmon-induced TPACS enhancement in ensembles of colloidal QDs. Moreover, the enhancement of QD PL near PNPs under TPE may be a result of the Purcell effect, and it is still an important task to evaluate the contribution of direct TPACS enhancement to the total enhancement of TPE PL of excitons in QDs.

Here, we have specially studied the TPACS of excitons in thin-film hybrid structures based on QDs and gold PNPs and have found effective enhancement of TPACS by a factor of up to 12. For this purpose, we used the recently reported technique for measuring the TPACSs of single-exciton states in QDs by measuring the saturation of TPE PL.[4] It allowed us to distinguish between the TPACS enhancement and effects of plasmons on the spontaneous radiation rate, including the Purcell effect and metal-induced energy transfer from the emitting state of excitons. As a result, we have shown that an increase in the effective TPACS is a result of the nonlinear interaction of the excitons in QDs with plasmons linearly induced in PNPs.

Experimental

Synthesis of nanomaterials

The QDs were synthesized using the procedures reported earlier (see details in the ESI).[27] Their size was about 4.5 nm, as reported previously (Fig. S1 in the ESI).[4,22] Gold nanospheres (GNSs) were synthesized by the $NaBH_4$ reduction method.[28] An $HAuCl_4$ solution was prepared by diluting 0.68 mg of $HAuCl_4$ (Sigma Aldrich, catalog no. 254169) in 3 ml of deionized ice-cold water (4°C). A $NaBH_4$ solution was prepared by diluting 0.0454 mg of $NaBH_4$ (Sigma Aldrich, catalog no. 71321) in 1 ml of ice-cold water (4°C). Then, 0.75 ml of the $HAuCl_4$ solution was placed in a 2-ml microtube with magnetic stirring at 750 rpm, and 0.25 ml of the reducing agent ($NaBH_4$ solution) was added drop by drop with continuous stirring at a temperature of about 4°C. The stirring was continued for another 10 min for complete homogenization. Before use, the GNS solution was stored in the dark at a temperature of 4°C for 1 week. The GNRs were synthesized as described earlier (see details in the ESI).[29]

View Article Online DOI: 10.1039/D0NR08937F

Thin-film preparation

To fabricate a thin-film QD-in-PMMA hybrid structure, we employed the spin-coating method using a Model KW-4A Spin Coater. Poly(methyl methacrylate) (PMMA) with an average molecular weight of □120,000 as measured by GPC (Sigma Aldrich, 182230) was mixed with QDs in a toluene solution with a final QD concentration of 10^{-6} M and a PMMA weight concentration of 1.2 wt%. This mixed solution was spin-coated onto the glass substrate at 1000 rpm. The final film thickness was 20 nm as measured by atomic force microscopy. To calculate the near-surface density of QDs in the PMMA, film we assumed that the ratio of the number of QDs to the weight of PMMA was the same in the initial solution and in the spin-coated film. We also assumed that the density of PMMA film was the same as the density of bulk PMMA (1.18 g/cm^3). Thus, for a PMMA film with a thickness of 20 nm, the QD near-surface density was about $1.36 \cdot 10^{11}$ cm^{-2}, which corresponded to 735 nm^2 of PMMA film surface per QD in the film. The positions of the QDs in the PMMA film were random.

Photoluminescence measurements

The PL signals were measured using a setup based on a Tsunami femtosecond laser (Spectra Physics) with a pulse repetition rate of 80 MHz, tunable pulse duration of up to 60 fs, and pulse energy of up to 20 nJ. Additionally, a laser pulse selector module (Model 3980-6M, Spectra Physics) was used to reduce the pulse repetition rate to 1.6 MHz in the case of time-resolved measurement; however, this module also reduced the pulse duration to 300 fs and pulse energy to 4 nJ per pulse. The PL signal was excited and collected by a confocal optical scheme using a lens with a focusing length of 35 mm, the waist of the focused beam was approximately 25 μm. The PL signal was recorded by means of an M266 monochromator/spectrograph (Solar Laser Systems) with a Hamamatsu high-sensitivity CCD module installed. A PD-050-CTD detector (Micro Photon Devices) with a resolution of up to 50 ps connected to a Pico Harp 300 electronic photon counting module (Pico Quant) was additionally connected to the monochromator/spectrograph to measure the PL decay kinetics by the method of time-correlated

single-photon counting. The setup allowed PL time-resolved measurement with a time resolution of down to 150 ps. We tuned the pulse energy using a polarizing laser pulse attenuator dividing the laser beam into two beams (p-polarized and s-polarized ones). We used only the p-polarized beam. Intensity-weighted averaging was used for the calculation of the PL lifetime for the multiexponential kinetics (see ESI for details).

The maximum laser intensity used was limited by the heating of the GNRs, because their linear absorption cross-section was of the order of 10^{-13} cm^2.[30,31] Earlier, El-Sayed and coworkers found that an adsorbed energy threshold of 60 ± 20 fJ is required to melt a nanorod using ultrafast pulses,[32] and in another study the energy flux value of up to 5 J/cm^2 was found safe for the GNR structural stability.[33] Thus, to meet both of these limitations, we used the energy flux values lower than 5 J/cm^2 in all experiments.

Numerical simulations

To simulate the near-field distribution in the vicinity of PNPs excited by an external field we used the finite elements method in an electromagnetic module of the COMSOL Multiphysics 5.5 software. The simulated plane wave was linearly polarized according to the experimental conditions. The refractive index of PMMA was set to the known value of 1.484 for the excitation range. The wavelength-dependent values of the complex refractive index of gold was taken from the study where it was calculated using the Lorentz–Drude model.[34] Because GNRs were covered with cetyltrimethylammoniumbromide (CTAB), we also added this layer to our model. The CTAB layer thickness was assumed to be 3.4 nm, on the basis of reports where it was measured, and its refractive index was set to the known value of 1.435.[35,36]

Results and discussion

To investigate the effect of plasmons on the TPACS of excitons in QD–PNP hybrids, we examined two distinct cases. In the first one, there was a strong overlap between the plasmon band and excitation wavelength (Fig. 1a). Here, we used GNRs with an extinction maximum at 790 nm corresponding to the dipole longitudinal mode of localized plasmons and QDs with the PL spectrum maximum at 560 nm as emitters (Figure 1a). GNRs had a spherocylindrical shape with a diameter of 12.5 nm and a length of 50 nm (Fig. S2 in the ESI). In the second case, a large overlap between the plasmon and QD PL bands and no overlap with the excitation wavelength were ensured by using GNSs. The GNS extinction maximum was at 530 nm (Fig. 1a), which corresponded to a diameter of about 30 nm.[37–39] In both cases, CdSe/(ZnS/CdS/ZnS) core/multishell QDs with a PL spectrum maximum in a hexane solution at 560 nm (Fig. 1a), the PL lifetime of 35 ns (Fig. 1b), and the QY of 90% were used.

For each experiment, we fabricated three thin-film hybrid structures consisting of QDs in a 20-nm-thick PMMA layer (Fig. 2a). We chose this thickness because it had been previously shown to be within the optimum range for the maximum PL enhancement in QDs located near PNPs.[10,40] Therefore, in a

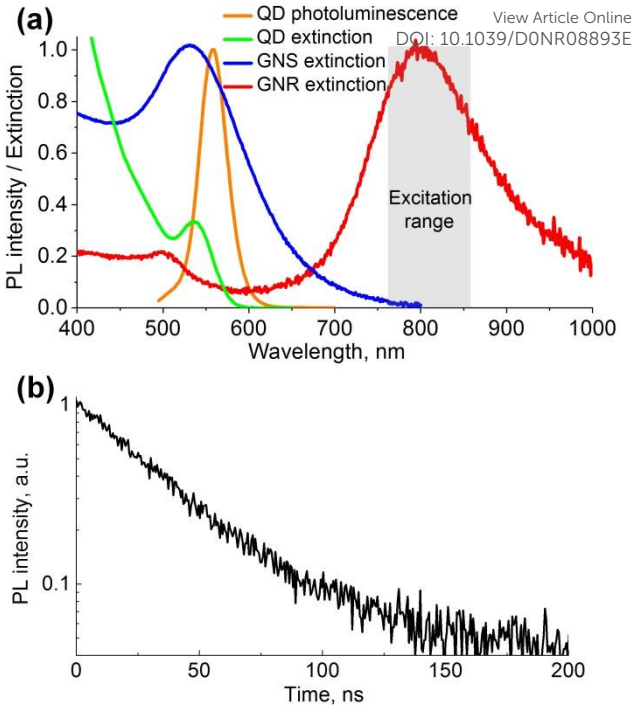

Fig. 1 Optical properties of the nanoparticles used. (a) The QD TPE PL spectrum (orange line), QD one-photon extinction spectrum (green line), GNS one-photon extinction spectrum (blue line), and GNR one-photon extinction spectrum (red line); the transparent gray bar shows the spectral range of the laser excitation. (b) The TPE PL decay for QDs in a hexane solution.

thicker layer, too many QDs would have been unable to interact with PNPs. On the other hand, in too thin a PMMA film, the amount of QDs in the focal volume would have been strongly decreased and the signal-to-noise ratio would have been too low under TPE. After fabrication of the initial 20-nm QD-in-PMMA layers, some of these samples were covered with the GNSs or GNRs by dropping aqueous PNP solutions and drying the samples, which resulted in the formation of disordered surface films (Fig. 2a). Taking into account that the extinction cross-sections of PNPs of the sizes used here are of the order from 10^{-13} to 10^{-12} cm^2,[30,31] the surface density of the GNRs was estimated to be about 10^{11} to 10^{12} cm^{-2}, which ensured the full covering of the film surface by both PNP types. Afterwards, the TPACS of excitons in the fabricated hybrid structures was estimated.

TPACS is the main parameter that reflects the TPE efficiency regardless of the amplitude of the excitation field. Previously, we showed that the TPE PL saturation measurements in the spectra of only single-exciton QD states allow finding the TPACS in QD ensembles without prior knowledge of their concentration and QY.[4] To describe the saturation of TPE PL in QDs, we used the equation that expressed this process as a function of excitation intensity. It was found that the intensity-weighted average PL lifetime of QDs in a PMMA film is 25 ns (Fig. 2b). With this value, we calculated the PL intensity *F* using the previously derived dependence of *F* on the peak excitation

View Article Online
DOI: 10.1039/D0NR08893E

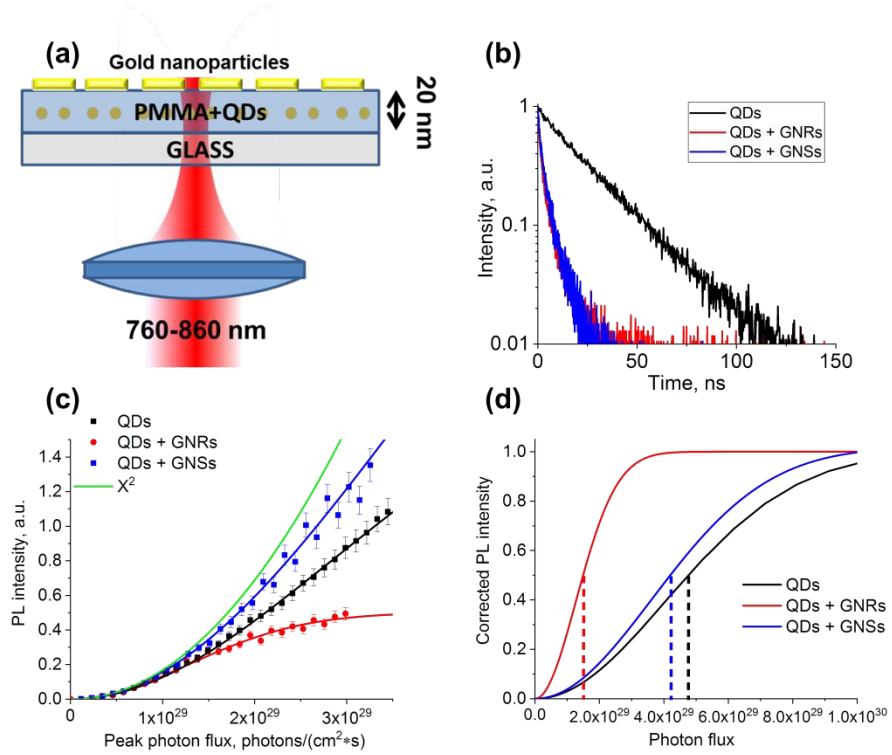

Fig. 2 The scheme of the experiment and experimental results and calculations for the QD–PNP samples. (a) The scheme of the experiment. (b) The TPE PL decays for QDs in thin PMMA films in the presence of GNRs (red line) and GNSs (blue line) as compared to the TPE PL decay in the samples without PNPs (black line). (c) Characteristic dependences of the TPE PL intensity on the excitation intensity (at a wavelength of 790 nm) for QDs in thin-film hybrid structures without PNPs (black squares) and in the presence of GNRs (red circles) and GNSs (blue squares). The green line represents a pure quadratic dependence. The other lines are the results of the TPE PL saturation fitting by eqn (1). (d) TPE PL saturation curves from panel (c) recalculated for single-pulse excitation, with deflection points indicated by dashed lines.

intensity I_0 [photons/(s·cm^2)] and taking into account the laser pulse duration, laser period T, and PL lifetime τ_{lum}:

$$F(I_0) = N \cdot \Phi \cdot g \cdot \frac{\left(1 - e^{-T/\tau_{lum}}\right) \cdot \left(1 - e^{-\sigma^{(2)} \cdot I_0^2 \cdot \tau_{las}}\right)}{\left(2 - e^{-T/\tau_{lum}} \cdot e^{-\sigma^{(2)} \cdot I_0^2 \cdot \tau_{las}} - e^{-T/\tau_{lum}}\right)}, \quad (1)$$

where $\sigma^{(2)}$ is the TPACS, N is the number of QDs in the excited volume, Φ is the PL QY, and g is the factor of PL collection efficiency. However, when we placed the QD near the PNP, the excitons interacted not only with external far-field $\boldsymbol{E}_0$, but also with the plasmon-induced near-field. Thus, if we still use the easily measurable far-field intensity I_0 (eqn (1)) we should use the effective TPACS ($\sigma_{eff}^{(2)}$) instead of $\sigma^{(2)}$ to account for the effect of plasmons on the TPA of excitons in QDs:

$$\sigma_{eff}^{(2)} = \alpha^2 \cdot \sigma^{(2)}, \quad (2)$$

where α is a factor that reflects the change in the inflection point of the saturation curves (Fig. 2c). It should be noted that, in the presence of PNPs, the QD PL lifetime was drastically shortened from 25 ns to about 3 ns for both GNSs (the blue line in Fig. 2b) and GNRs (the red line in Fig. 2b). This finding indicates that the plasmon–exciton interaction leads to modification of the radiative and nonradiative recombination rates of excitons in the QD and, hence, the PL QY may be strongly affected. Fortunately, the change in the PL QY is of no importance for the measurement of the $\sigma_{eff}^{(2)}$ using the TPE PL saturation technique, where only the excitation field and TPACS value can affect the saturation threshold. Indeed, the saturation threshold is characterized only by the point of inflection of the dependence of PL intensity F on the excitation intensity I_0. Thus, the first three terms of eqn (1) do not affect this point, and we do not need to know the value of the exciton PL QY. This fact sufficiently simplifies the TPACS measurement process, because, in the case of optically thin samples, the PL QY measurement is very difficult. However, the PL lifetime parameter τ_{lum} is very important for calculations, if the repetition rate of the excitation source is comparable with it. We used an 80 MHz excitation source because this repetition rate is one of the most common for infrared mode-locked ultrafast lasers and allow obtaining a quasi-continuous PL signal, which is important for bioimaging and biosensing. Thus, the PL lifetime was an important parameter for the calculations.

We experimentally obtained the TPE PL saturation curves for QDs in PMMA without PNPs and in the presence of GNSs (blue dots in Fig. 2c) or GNRs (red dots in Fig. 2c) at the excitation wavelength of 790 nm. The plots in Fig. 2c were equaled for low-intensity excitation to show that all of them initially followed a square dependence (the green line in Fig. 2c). We equaled the data in Fig. 2c because of the high variance of the absolute value of the PL intensity between samples, and even between different points on the sample surface. We believe that this is because of the non-homogenous distribution of QDs in the PMMA film. In turn, the variation of the position of the saturation threshold between different experimental regions of interest was low enough to calculate the TPACS with a

View Article Online
DOI: 10.1039/D0NR08893E

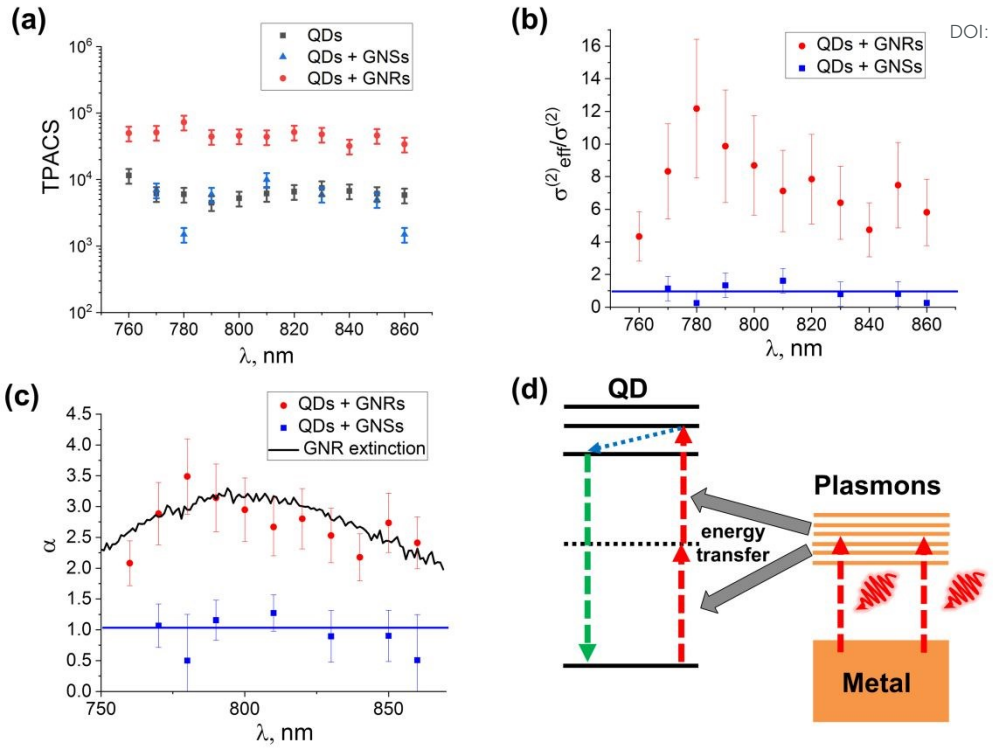

Fig. 3 Effect of GNRs on the exciton TPACS in QDs. (a) The measured TPACS of excitons in QDs in the absence of PNPs (black squares), QDs near GNSs (blue triangles), and QDs near GNRs (red circles). (b) The calculated change in the effective TPACS of excitons near GNRs (red circles) or GNSs (blue squares). (c) The calculated increase in the near-field intensity of plasmon modes in PNPs compared to the intensity of far-field (GNRs, red circles; GNSs, blue squares); for comparison, the experimental GNR extinction spectrum (black line) is also shown. (d) The scheme of the plasmon–exciton interaction under external excitation.

reasonable error. This is because the position of the saturation threshold does not depend on the number of emitters, QY, or overall PL intensity, as it follows from eqn (1). During the measurement yielding the saturation curve, we did not change the position of the objective lens; hence, the inhomogeneous distribution did not affect any saturation curve measured.

One can see from Fig. 2c that at higher excitation intensities the plots deviate from the square dependence, which shows a tendency to saturation. The most pronounced TPE PL saturation was observed for QDs in the presence of GNRs, which can be explained by the increase in $\sigma_{eff}^{(2)}$ compared to $\sigma^{(2)}$. It is noteworthy that a much weaker effect of TPE saturation was observed for QDs located near GNSs than for QDs in the absence of PNPs; this can be attributed to the alteration of the QD PL lifetime. Indeed, the PL lifetime of 25 ns for QDs in PMMA without PNPs considerably affects the TPE saturation threshold by shifting it to the lower excitation intensity (eqn (1)). Thus, if there had been no TPE enhancement for QDs in the vicinity of GNSs with a PL lifetime of 3 ns, this threshold would have been observed at higher intensities than without any PNPs. To visualize this effect, in Fig. 2d, we plotted saturation curves from Fig. 2c which were corrected for the single-pulse excitation ($T \rightarrow \infty$) with equaled first three terms of eqn (1). In this case, one can see that the inflection for QDs near GNSs is observed at lower excitation intensity than for QDs in the absence of PNPs.

Then, by fitting the experimental dependences with eqn (1), we found both $\sigma^{(2)}$ using the saturation curve for the case of QDs without PNPs (the black line in Fig. 2c) and $\sigma_{eff}^{(2)}$ using the saturation curves for the cases of QDs covered with GNRs (the red line in Fig. 2c) and GNSs (the blue line in Fig. 2c). We repeated these measurements for the wavelengths of excitation from 760 nm to 860 nm and found both $\sigma^{(2)}$ and $\sigma_{eff}^{(2)}$. The results are presented in Fig. 3a. One can see that the $\sigma_{eff}^{(2)}$ values for QDs near GNRs were much higher than $\sigma^{(2)}$, but the $\sigma_{eff}^{(2)}$ values for QDs near GNSs were equal to or even smaller than $\sigma^{(2)}$ (we will discuss this finding below). To show this clearly, we divided $\sigma_{eff}^{(2)}$ by $\sigma^{(2)}$ and plotted the resulting values in Fig. 3b. The case of QDs near GNRs demonstrates a strong, 12-fold enhancement of $\sigma_{eff}^{(2)}$. Unlike GNRs, GNSs are unable to interact with radiation at excitation wavelengths (760-860 nm). At the same time, GNSs have a wide plasmon resonance band in the spectral region of QD PL, which is also directly related to an increase in the density of photon states within this spectral range near the GNS surface, as it is well-known. Thus, GNSs are incapable of affecting the two-photon excitation of QDs, but, at the same time, they are potentially capable of implementing the Purcell effect for nearby QDs. In addition, these resonance conditions can also lead to nonradiative energy transfer from the QDs to the GNSs. As we can see from Fig. 2b, the lifetime shortening was almost the same for QDs near GNRs and near GNSs. This indicates that in both cases the Purcell effect and PL quenching (due to the nonradiative energy transfer) can occur, because both GNRs and GNSs have plasmon modes at the wavelength of the QD PL (Fig. 1a). However, the main difference

View Article Online
DOI: 10.1039/D0NR08897F

between GNRs and GNSs is that GNRs can interact with external radiation and GNSs cannot. As a result, this difference indicates that the effect of GNRs on the TPACS is most likely to be related to the implementation of plasmon oscillations under the effect of external near-infrared radiation, which is impossible in the GNS system. Additionally, the TPE PL saturation technique allowed us not to be concerned about the change in the QY of excitons near PNPs. Because the plasmon-induced PL quenching and Purcell effect commonly affect the QY of the fluorophore, our technique allows us to exclude them from consideration.

It is interesting that the observed TPACS enhancement was maximum at the excitation wavelength of 780 nm (Fig. 3b), which is very close to the maximum of the GNR extinction spectrum (790 nm). Indeed, we can account for the plasmon-induced change in the inflection point position without involving the $\sigma_{eff}^{(2)}$ value, by using the effective near-field intensity I instead of far-field intensity I_0:

$$I = \alpha \cdot I_0, \quad (3)$$

The intensity of the generation of plasmons in PNPs under external excitation at different wavelengths is proportional to the extinction spectrum intensity. We plotted the dependence of α on the excitation wavelength (Fig. 3c, red dots), and it is evident that this dependence closely follows the outline of the GNR extinction band (Fig. 3a, the black line). This indicates that the observed enhancement was a result of the interaction of excitons with longitudinal plasmon modes in GNRs, which had the maximum generation efficiency at 790 nm. The smaller the overlap between the excitation and GNR extinction bands, the less efficient the interaction of the external field with plasmon modes, and lower enhancement was obtained in the experiments.

Commonly, two-photon excitation of excitons in QDs is performed using ultrashort pulse lasers, because of their ultrahigh peak excitation intensities. Thus, under such an experimental arrangement this system can be considered as a nonlinear interaction of the dipole (exciton) with an external electromagnetic field, which has the temporal and spatial characteristics of the laser pulse used.[4] However, in the hybrid plasmon-exciton samples fabricated in this study, the situation was more complex. Under our experimental conditions, an external field initiated by an ultrashort laser pulse interacts simultaneously both with excitons in QDs and with plasmons in gold nanorods. In contrast to the two-photon interaction of photons with excitons in QDs, the interaction of photons with plasmons is linear, which leads to the excitation of a large number of plasmons simultaneously in one nanorod. One of the traditional ways to treat this system is consideration of the interaction of excitons with the resulting nearfield alone, which is a result of interference of the nearfield of plasmon oscillations and the external field, as if they both are steady-state.[22,25] This approach is well justified if the plasmon lifetime is negligible compared to the pulse duration, facilitating the calculation of the absorption efficiency because the dipole-dipole interaction between the plasmon and the exciton is reduced to the interaction of the exciton with the resulting nearfield. However, using the ultrashort laser pulses for excitation, we should not only take into account the temporal profile of the laser pulse (in our case, it is close to the square of the hyperbolic secant function),[4] but also consider plasmon oscillations as a damped oscillator the mode of which also has a temporal profile. Moreover, there is the difference between the physical interpretations of the interactions of an exciton with an external field and a nearfield of plasmon modes. External excitation can be represented as a flux of photons and has the certain direction of the Poynting vector, while the nearfield of plasmons is determined only by the mode of the resultant oscillations and does not require photons for the description. These reasons complicate the using of the above-mentioned approach for theoretical estimations.

In this study, we propose an alternative approach for the consideration of this system, which, as we think, more accurately represents the physical nature of such a three-part (external field–plasmons–excitons) interaction and allows us to separately consider the plasmon-exciton interaction. In fact, we propose to consider the interactions of two dipoles (an exciton and the longitudinal plasmon mode of a gold nanorod) with the field of external radiation and with each other separately. This means that the plasmons excited in the GNR linearly can further transfer the energy to the exciton in a QD through dipole-dipole interaction. However, the energy of plasmons in the GNR induced by the external field with the wavelength of 790 nm (1.57 eV) was not enough to linearly transfer the energy to the exciton in the QD (with a band gap of 2.21 eV). This indicates that in our system the nonlinear (two-quantum) plasmon-exciton interaction occurred (Fig. 3d). This also means that we need two plasmons (two quanta of the longitudinal plasmon mode) to excite one exciton in the QD through dipole-dipole energy transfer from the GNR. The description of the linear dipole-dipole interaction involves the polarizability of the acceptor dipole, but in our case to calculate the probability of the transfer of the energy of two plasmons to one exciton, we need its nonlinear polarizability (hyperpolarizability). According to the semiclassical general description, the power transferred to the exciton in a QD due to this type of nonlinear dipole–dipole interaction can be estimated by replacement of the linear dipole moment with the fourth term of its full mathematical expansion in the well-known equation:[41,42]

$$P(\omega,t,\boldsymbol{r}_{QD}) = \frac{\omega}{12} \cdot Im\{\gamma_{QD}\} \cdot |\boldsymbol{e}_{QD} \cdot \boldsymbol{E}_{pl}(t,\boldsymbol{r}_{QD})|^4, \quad (4)$$

where ω is the frequency corresponding to the energy of plasmon, $\mathbf{e}_{QD}$ is the exciton dipole orientation vector, $\boldsymbol{E}_{pl}(\boldsymbol{r}_{QD})$ is a plasmon-induced near-field at the position of the QD ($\boldsymbol{r}_{QD}$), and γ_{QD} is the second hyperpolarizability of excitons, whose averaged imaginary part can be derived from $\sigma^{(2)}$:[43]

$$Im\{\gamma_{QD}\} \approx \frac{2n^2 \cdot c^2 \cdot \varepsilon_0}{3\hbar \cdot \omega^2} \sigma^{(2)}, \quad (5)$$

where n is the refractive index of the medium, ε_0 is the vacuum permittivity, and c is the speed of light. If the amplitude of $\boldsymbol{E}_{pl}$, which is a result of the interference between the plasmon near-field mode and the external far-field $\boldsymbol{E}_0$, is higher than $|\boldsymbol{E}_0|$, then

View Article Online
DOI: 10.1039/D0NR08893E

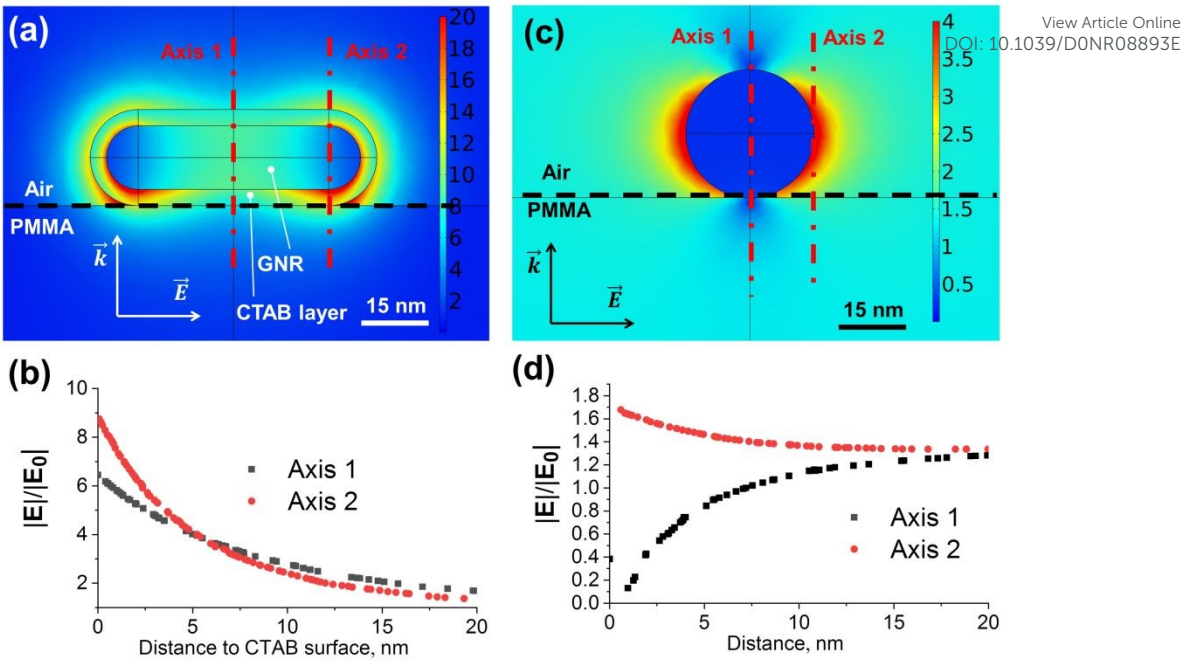

Fig. 4 The calculated near-field distribution in the vicinity of PNPs on top of the PMMA film under excitation at a wavelength of 780 nm. (a) The simulated field distribution near a single GNR. (b) The calculated dependence of the field amplitude increase near the GNR on the distance from the PMMA surface for two x-axis positions (see panel a). (c) The simulated field distribution near a single GNS. (d) The calculated dependence of the field amplitude increase (or decrease) near the GNS on the distance from the PMMA surface for two x-axis positions (see panel c).

the plasmon energy will be nonlinearly transferred to excitons in QDs. The reverse process of energy transfer is impossible because the energies of exciton transitions are much higher than the energy of plasmons. This leads to the one-way "pumping" of excitons by plasmons and further increases the excitation efficiency of excitons in QDs near GNRs. Because the plasmons are excited linearly by the external laser field and PNPs have extremely high linear absorption cross-sections,[44] this "pumping" is not accompanied by noticeable depletion of plasmon states.

We also note that the efficiencies of the excitation of excitons by plasmons and the external wave may be different at equal field amplitudes due to the differences between near-field and far-field orientations, and because the plasmon lifetime is only about 10–20 fs.[45] However, during the lifetime of plasmons, they can, together with the external excitation, additionally nonlinearly "pump" excitons in QDs if the interference between their near-field and far-field is positive. From eqn (1) one can see that the position of the inflection point is determined only by the value of the square root of the energy absorbed during the laser pulse, $(\sigma^{(2)} \cdot I_0^2 \cdot \tau_{las})^{1/2}$. Thus, the value of α^2, which is equal to the relative change in the effective TPACS (eqn (2)), is proportional to the ratio of the energy absorbed by excitons near the PNP to the energy absorbed by the QD in the absence of PNPs:

$$\alpha^2 \propto \frac{\iint |\boldsymbol{e}_{QD} \cdot \boldsymbol{E}_{pl}(t, \boldsymbol{r}_{QD})|^4 \cdot dt \cdot d\boldsymbol{r}}{\tau_{las} \cdot \int |\boldsymbol{e}_{QD} \cdot \boldsymbol{E}_0|^4 \cdot d\boldsymbol{r}}. \quad (6)$$

To support that the interaction of QDs with plasmons in GNRs may be very effective at distances of up to 20 nm, we simulated the plasmon modes in GNRs on the PMMA film. The direction of the external electromagnetic wave propagation was chosen perpendicular to the plane of the PMMA film, as it was in the experiment, and the wave frequency was selected to match the excitation wavelength of 780 nm. The shape of the GNRs used in simulation was determined earlier from their TEM images (see ESI).[29] To simulate the most efficient formation of longitudinal dipole plasmon modess in GNRs, we performed calculations for the polarization along the main GNR axis. The result of the interference of the plasmon-induced field with the excitation field is presented in Fig. 4a. It can be seen that the plasmon-induced near-field is stronger than the far-field in close proximity to the GNR. This indicates that, at short distances, plasmons may interact with QDs even more effectively than the external field alone. In Fig. 4b, we plotted the field increase in the PMMA matrix versus the distance from the PMMA surface for two axes (Axis 1 and Axis 2 in Fig. 4b), which coincided with the field propagation direction and intersected with the main axis of the GNR. One of these axes (Axis 1) passed through the center of the GNR, and the other (Axis 2) traversed the end of the GNR. From Fig. 4b one can see that, for distances up to 20 nm (the QD-in-PMMA layer thickness), the near-field increase factor varied from 1.3 to 9. In our samples, the GNR films were disordered, and, hence, the alignment of part of GNRs with the excitation polarization was accidental. We simulated the field distribution for different orientations of the polarization (up to perpendicaular or 90°) and plotted them in Fig. S4 in ESI. We found that, for most GNR orientations, the near-field may have been sufficiently high compared to the far-field, except for angles in the range of from 80° to 90°, at which negative interference occurred at short distances. In eqn (6), the factor of the TPACS enhancement is

proportional to the fourth order of the field amplitude. Thus, for efficient plasmon–exciton interaction, only a relatively small increase in the near-field amplitude is required. We calculated the $|\boldsymbol{E}_{pl}|^4/|\boldsymbol{E}_0|^4$ averaged over the 20-nm-thick PMMA volume under the GNR surface and plotted it in Fig. S5 (ESI) as the dependence on the angle between the GNR main axis and $\boldsymbol{E}_0$ direction. The value averaged over the angles $|\boldsymbol{E}_{pl}|^4/|\boldsymbol{E}_0|^4$ was, therefore, □100. In fact, this estimation is true only for the steady-state excitation mode, and the time profiles of plasmon modes should be taken into account for more accurate estimation. Thus, our evaluation yields only the upper bound for the maximum possible TPACS amplification; in practice, it was reduced by the exciton dipole orientation distribution and ultrafast damping of plasmon modes. However, this estimation supports our conclusion that the experimentally obtained increase in the $\sigma_{eff}^{(2)}$ of excitons in the QDs near GNRs is the result of the interaction with the longitudinal dipole mode of localized plasmons in GNRs.

To show that the process of nonlinear interaction of excitons with plasmons in GNSs was negligible at the same excitation conditions, we simulated a GNS on the PMMA surface (Fig. 4c). One can see that the plasmon-induced field was distributed mainly on the left and right, but the interference was negative in the matrix directly under the GNS. We plotted the field increase versus the distance from the PMMA surface in the PMMA matrix for two axes (Axis 1 and Axis 2 in Fig. 4d), which coincided with the field propagation direction. One can see that, for some positions, the interaction of QDs with plasmons may be negative and, hence, the $\sigma_{eff}^{(2)}$ may be even lower than $\sigma^{(2)}$. We believe that this is the reason why some experimentally measured $\sigma_{eff}^{(2)}$ values were lower than $\sigma^{(2)}$ (Fig. 3a). However, for most QD positions under GNS, the near-field is, on average, not much different from the far-field, and this is why, in most cases, we observed negligible changes in the $\sigma_{eff}^{(2)}$ of excitons in QDs near GNSs.

Conclusions

In this study, we investigated the effect of the nonlinear plasmon–exciton interaction on the effective TPACS of excitons in QDs located close to PNPs, regardless of the changes in the spontaneous radiation lifetime and QY, as well as of the Purcell effect. To exclude the effect of the changes in the PL QY or PL lifetime, we used the TPE PL saturation technique, which allowed direct measurement of the TPACS of excitons in QDs. Additionally, we investigated the effect of spectral overlapping between the PNP plasmon band, QD PL band, and excitation wavelength on the effective TPACS. For this purpose, two types of PNPs were used: the first one, GNRs with a plasmon band strongly overlapping with the excitation wavelengths and not overlapping with the QD PL, and the second one, GNSs with a plasmon band matching the QD PL band but not overlapping with the excitation wavelengths. The fabricated sandwich-like thin hybrid structures consisted of a 20-nm PMMA film with incorporated QDs and a layer of gold PNPs, which enabled TPE in the spectral range of 760–860 nm. The effective TPACSs of the QDs in both structures were evaluated by analysing the PL saturation curves in the TPE mode. As a result, we found that, in the case of GNSs, there was no increase in the effective TPACS compared to the QD-in-PMMA films not covered with PNPs, whereas a 12-fold increase in the effective TPACS was achieved by using GNRs. Furthermore, we demonstrated that the increase in the effective TPACS was higher in the case of a larger overlap between the excitation wavelength and plasmon band. We, therefore, believe that the obtained increase was a result of the nonlinear nanoscale interaction of the longitudinal dipole plasmon modes in GNRs with excitons in QDs. This conclusion was supported by numerical simulation of the field distribution near GNRs and GNSs of the same shape and size as those used in the experiment. The results of the simulation are in good agreement with the experimental data and support our conclusions. Thus, we have developed an approach to directly increasing the effective TPACS of the excitons in QDs by inducing nonlinear near-field interaction between absorptive exciton transitions in QDs and plasmon modes in PNPs. The TPE PL method used makes it possible to accurately quantify the plasmon-induced TPACS enhancement, not only regardless of the presence or absence of the Purcell effect, but also without prior knowledge of the QD concentration, PL QY, or exciton recombination rates. We believe that the results of our study will expand the applications of TPE of plasmon–exciton hybrid structures in multiphoton sensing and bioimaging, photodynamic therapy, and fabrication of nonlinear optical photodetectors.

Conflicts of interest

There are no conflicts to declare.

Acknowledgements

V.K. acknowledges support from the Russian Science Foundation (Grant No. 18-72-10143) for the part of the study related to investigation of the effects of PNPs on the effective TPACS of excitons in QDs and numerical simulations of these effects. Support from the Ministry of Education and Science of the Russian Federation (Grant No. 14.Y26.31.0011) for the part of this study related to the synthesis and fonctionnalisation of the QDs and engineering of hybrid QD-GNR materials is also acknowledged. Y.R. acknowledges the support from the Basque Government (grant no. IT1164-19). Y.R. and M.G. acknowledge the support from the Spanish MINECO (PID2019-111772RB-I00). I.N. acknowledges the Ministry of Higher Education, Research and Innovation of the French Republic and Université de Reims Champagne-Ardenne. The authors thank Mrs. Daria Dyagileva for the help with preparation of the thin QD-in-PMMA films and Mr. Vladimir Ushakov for the help with technical preparation of the manuscript.

References

1 R. Gui, H. Jin, Z. Wang and L. Tan, *Coord. Chem. Rev.*, 2017, **338**, 141–185.

2 V. Dneprovskii, M. Kozlova, A. Smirnov and T. Wumaier, *Phys. E Low-dimensional Syst. Nanostructures*, 2012, **44**, 1920–1923.
3 R. Scott, A. W. Achtstein, A. Prudnikau, A. Antanovich, S. Christodoulou, I. Moreels, M. Artemyev and U. Woggon, *Nano Lett.*, 2015, **15**, 4985–4992.
4 V. Krivenkov, P. S. Samokhvalov, D. Dyagileva, A. Karaulov and I. R. Nabiev, *ACS Photonics*, 2020, **7**, 831–836.
5 K. T. Yong, G. Xu and I. Roy, *Chem. Commun.*, 2011, **47**, 2901–2903.
6 L. M. Maestro, J. E. Ramírez-Hernández, N. Bogdan, J. A. Capobianco, F. Vetrone, J. G. Solé and D. Jaque, *Nanoscale*, 2012, **4**, 298–302.
7 H. Hafian, A. Sukhanova, M. Turini, P. Chames, D. Baty, M. Pluot, J. H. M. Cohen, I. Nabiev and J.-M. Millot, *Nanomedicine*, 2014, **10**, 1701–9.
8 V. Krivenkov, P. Samokhvalov and I. Nabiev, *Biosens. Bioelectron.*, 2019, **137**, 117–122.
9 A. M. Smirnov, M. V. Kozlova and V. S. Dneprovskii, *Opt. Spectrosc.*, 2016, **120**, 472–476.
10 O. Kulakovich, N. Strekal, A. Yaroshevich, S. Maskevich, S. Gaponenko, I. Nabiev, U. Woggon and M. Artemyev, *Nano Lett.*, 2002, **2**, 1449–1452.
11 L. Trotsiuk, A. Muravitskaya, O. Kulakovich, D. Guzatov, A. Ramanenka, Y. Kelestemur, H. V Demir and S. Gaponenko, *Nanotechnology*, 2020, **31**, 105201.
12 I. Gryczynski, J. Malicka, Yibing Shen, A. Zygmunt Gryczynski and J. R. Lakowicz, *J. Phys. Chem. B*, 2002, **106**, 2191–2195.
13 W. Wenseleers, F. Stellacci, T. Meyer-Friedrichsen, T. Mangel, C. A. Bauer, S. J. K. Pond, S. R. Marder and J. W. Perry, *J. Phys. Chem. B*, 2002, **106**, 6853–6863.
14 I. Cohanoschi, S. Yao, K. D. Belfield and F. E. Hernández, *J. Appl. Phys.*, 2007, **101**, 086112.
15 S. T. Sivapalan, J. H. Vella, T. K. Yang, M. J. Dalton, J. E. Haley, T. M. Cooper, A. M. Urbas, L.-S. Tan and C. J. Murphy, *J. Phys. Chem. Lett.*, 2013, **4**, 749–752.
16 O. S. Ojambati, R. Chikkaraddy, W. M. Deacon, J. Huang, D. Wright and J. J. Baumberg, *Nano Lett.*, 2020, **20**, 4653–4658.
17 D. F. Zhang, S. Li, Q. H. Xu and Y. Cao, *Langmuir*, 2020, **36**, 4721–4727.
18 T. Zhao, K. Yu, L. Li, T. Zhang, Z. Guan, N. Gao, P. Yuan, S. Li, S. Q. Yao, Q.-H. Xu and G. Q. Xu, *ACS Appl. Mater. Interfaces*, 2014, **6**, 2700–2708.
19 D. Dovzhenko, V. Krivenkov, I. Kryukova, P. Samokhvalov, A. Karaulov and I. Nabiev, *Opt. Lett.*, 2020, **45**, 5364–5367.
20 V. Giannini, A. I. Fernández-Domínguez, S. C. Heck and S. A. Maier, *Chem. Rev.*, 2011, 111, 3888–3912.
21 F. Tam, G. P. Goodrich, B. R. Johnson and N. J. Halas, *Nano Lett.*, 2007, **7**, 496–501.
22 V. Krivenkov, D. Dyagileva, P. Samokhvalov, I. Nabiev and Y. Rakovich, *Ann. Phys.*, 2020, **532**, 2000236.
23 A. M. Craciun, M. Focsan, L. Gaina and S. Astilean, *Dye. Pigment.*, 2017, **136**, 24–30.
24 S. Xiao, H. Gong, X. Su, J. Han, Y. Han, A. Mutian Chen and Ququan Wang, *J. Phys. Chem. C*, 2007, **111**, 10185–10189.
25 W. Zhang, M. Caldarola, X. Lu and M. Orrit, *ACS Photonics*, 2018, **5**, 2960–2968.
26 S.-H. Gong, S. Kim, J.-H. Kim, J.-H. Cho and Y.-H. Cho, *ACS Photonics*, 2018, **5**, 711–717.
27 P. Samokhvalov, P. Linkov, J. Michel, M. Molinari and I. Nabiev, *Proc. SPIE*, 2014, 8955, 89550S-89550S–7.
28 M. Iqbal, G. Usanase, K. Oulmi, F. Aberkane, T. Bendaikha, H. Fessi, N. Zine, G. Agusti, E. S. Errachid and A. Elaissari, *Mater. Res. Bull.*, 2016, **79**, 97–104.
29 D. Melnikau, R. Esteban, D. Savateeva, A. Sa, M. Grzelczak, J. Aizpurua, Y. P. Rakovich, A. Sánchez-Iglesias, M. Grzelczak, M. K. Schmidt, L. M. Liz-Marzán, J. Aizpurua and Y. P. Rakovich, *J. Phys. Chem. Lett.*, 2016, **7**, 354–362.
30 M. Alrahili, V. Savchuk, K. McNear and A. Pinchuk, *Sci. Rep.*, 2020, **10**, 1–9.
31 G. S. He, J. Zhu, K. T. Yong, A. Baev, H. X. Cai, R. Hu, Y. Cui, X. H. Zhang and P. N. Prasad, *J. Phys. Chem. C*, 2010, **114**, 2853–2860.
32 S. Link and M. A. Ei-Sayed, *J. Chem. Phys.*, 2001, **114**, 2362–2368.
33 H. Petrova, J. P. Juste, I. Pastoriza-Santos, G. V. Hartland, L. M. Liz-Marzán and P. Mulvaney, *Phys. Chem. Chem. Phys.*, 2006, **8**, 814–821.
34 A. D. Rakić, A. B. Djurišić, J. M. Elazar and M. L. Majewski, *Appl. Opt.*, 1998, **37**, 5271.
35 S. Gómez-Graña, F. Hubert, F. Testard, A. Guerrero-Martínez, I. Grillo, L. M. Liz-Marzán and O. Spalla, *Langmuir*, 2012, **28**, 1453–1459.
36 P. Kékicheff and O. Spalla, *Langmuir*, 1994, **10**, 1584–1591.
37 S. Link and M. A. El-Sayed, *J. Phys. Chem. B*, 1999, **103**, 4212–4217.
38 S. K. Ghosh, A. Pal, S. Kundu, S. Nath and T. Pal, *Chem. Phys. Lett.*, 2004, **395**, 366–372.
39 W. Haiss, N. T. K. Thanh, J. Aveyard and D. G. Fernig, *Anal. Chem.*, 2007, **79**, 4215–4221.
40 V. K. Komarala, Y. P. Rakovich, A. L. Bradley, S. J. Byrne, Y. K. Gun'ko, N. Gaponik and A. Eychmüller, *Appl. Phys. Lett.*, 2006, **89**, 253118.
41 K. Rustomji, M. Dubois, B. Kuhlmey, C. Martijn De Sterke, S. Enoch, R. Abdeddaim and J. Wenger, *Phys. Rev. X*, 2019, **9**, 011041.
42 C. L. Cortes and Z. Jacob, *Opt. Express*, 2018, 26, 19371–19387.
43 T. Kogej, D. Beljonne, F. Meyers, J. W. Perry, S. R. Marder and J. L. Brédas, *Chem. Phys. Lett.*, 1998, **298**, 1–6.
44 M. A. Van Dijk, A. L. Tchebotareva, M. Orrit, M. Lippitz, S. Berciaud, D. Lasne, L. Cognet and B. Lounis, *Phys. Chem. Chem. Phys.*, 2006, **8**, 3486–3495.
45 C. Sönnichsen, T. Franzl, T. Wilk, G. von Plessen, J. Feldmann, O. Wilson and P. Mulvaney, *Phys. Rev. Lett.*, 2002, **88**, 774021–774024.